

Computational Bottlenecks of Quantum Annealing

Sergey Knysh^{1,2,*}

¹QuAIL, NASA Ames Research Center, Moffett Field, California 94035, USA

²SGT Inc., 7701 Greenbelt Rd, Suite 400, Greenbelt, Maryland 20770, USA

A promising approach to solving hard binary optimization problems is quantum adiabatic annealing (QA) in a transverse magnetic field. An instantaneous ground state — initially a symmetric superposition of all possible assignments of N qubits — is closely tracked as it becomes more and more localized near the global minimum of the classical energy. Regions where the energy gap to excited states is small (e.g. at the phase transition) are the algorithm's bottlenecks. Here I show rigorously that even if the gap at the quantum critical point (QCP) scales as an inverse power of N , the problem can still be intractable. The model considered is that of Ising spins on a complete graph, with the additional restriction that the random matrix of interaction strengths J_{ik} has rank $p = 2$ (Hopfield network with two patterns). Exact solution reveals $\log N$ additional (to QCP) bottlenecks where the gap scales as a stretched exponential. Qualitative comparison with the NP-hard Sherrington-Kirkpatrick model (having full-rank J_{ik}) suggests that its annealing is adversely affected by the same phenomenon.

Quantum algorithms offer hope for tackling computer science problems that are intractable for classical computers¹. However, exponential speed-ups seen in, e.g. number factoring², have not materialized for more difficult NP-complete problems³. Those are targeted by quantum adiabatic annealing algorithm⁴⁻⁶. Any NP-hard problem can be recast as quadratic binary optimization. QA solves it by implementing a quantum Hamiltonian, written with the aid of Pauli matrices as

$$\hat{H} = -\frac{1}{2} \sum_{i,k=1}^N J_{ik} \hat{\sigma}_i^z \hat{\sigma}_k^z - \sum_{i=1}^N h_i \hat{\sigma}_i^z - \Gamma(t) \sum_{i=1}^N \hat{\sigma}_i^x. \quad (1)$$

Here the first two terms, diagonal in z -basis, encode the objective function. The last term represents the magnetic field in the transverse direction, which is decreased from $\Gamma(0) \gg 1$ to $\Gamma(T_{\text{ann}}) = 0$. The time T_{ann} needed by the algorithm is determined by a condition that the annealing rate is sufficiently low to inhibit non-adiabatic transitions:

$$d\Gamma/dt \ll \Delta E \cdot \Delta\Gamma. \quad (2)$$

These are most likely near points where the instantaneous gap to excited states ΔE attains a minimum as a function of Γ ; further, $\Delta\Gamma$ is defined as the width of the region where the gap remains comparable to its minimum value.

QA offers no worst-case guarantees on time complexity⁷, but initial assessments of *typical case*

complexity were optimistic. Both experimental⁸ and theoretical⁹ evidence pointed to performance improvement over simulated annealing for finite-dimensional glasses (of Edwards-Anderson type¹⁰). However, the empirical evidence in support of the theory — that quantum annealing simulated on classical computer beats its thermal counterpart — has recently been shown to be an artifact of discretization choice for the imaginary time¹¹. Early exact diagonalization studies also hinted at polynomially small gaps in constraint satisfaction problem on random hypergraphs¹², but that finding had been challenged by quantum Monte Carlo studies involving larger sizes¹³. Benchmarking of hardware implementation of QA, courtesy of D-Wave Systems, shows no improvement in the scaling of the performance^{14,15}. Whether that might be attributable to finite temperature at which the device operates or its intrinsic noise, is unclear at present¹⁶.

Statistical physics can help identify the asymptotic scaling of time complexity of QA. It has been linked to Ehrenfest type of underlying quantum phase transitions: For those of the first order, the gap becomes exponentially small in N at the transition point¹⁹⁻²². Less severe scaling, as a stretched exponential $\propto \exp(-cN^\epsilon)$, develops for continuous (2nd order) phase transition if the disorder is so strong that different parts of the system become critical at different times²³.

The most promising candidates for QA are problems with a bona fide second order phase transitions, where the disorder is irrelevant at the QCP. Scaling analysis described here suggests a polynomially small gap at the critical point of the archetypal spin glass: the Sherrington-Kirkpatrick (SK) model²⁴⁻²⁶. It has been pointed out^{9,27} that QA may still be doomed by the bottlenecks in the spin glass phase. Exponentially small gaps away from the critical point have been observed in simulations²⁸. Adequate theoretical description of this phenomenon proved challenging. A perturbative argument in support of this qualitative picture has been considered in ref. 27. However, the results were not borne out by more accurate analysis which took into account the extreme value statistics of energy levels²⁹.

The present manuscript sheds new light on the mechanism of tunneling bottlenecks in the spin glass phase. Exact, non-perturbative, methods are used to illustrate it for a simple model, but main findings are expected to be valid for quantum annealing of more realistic spin glasses. During annealing, the system must undergo a cascade of tunnelings at some specific values of $\Gamma_1, \Gamma_2, \dots$ in an approximate geometric progression. For finite system size, these bottlenecks are few, $O(\log N)$, and may

not even appear until N is sufficiently large, highlighting challenges of interpreting results of numerical studies. Bottlenecks also become progressively easier as $\Gamma \rightarrow 0$, counter to expectations that tunnelings are inhibited as the model becomes more classical. A related finding is that the time complexity of QA is exponential only in some fractional power of problem size: a mild improvement over more pessimistic estimates²⁷.

RESULTS

Summary. The spin glass phase, entered below some critical value of the transverse field Γ_c , is characterized by a large number of valleys. Often, this transition is abrupt, driven by competition between an extended state and a valley (localized state) with the lowest energy, as occurs in the random energy model^{20,21}. The exponentially small overlap between the two states determines the gap at the phase transition. However, even if new valleys develop in a continuous manner as Γ decreases, the spin glass phase may exhibit *transverse field chaos*. Intuitively, small changes in the transverse field may lead to the chaotic reordering of energy levels associated with these valleys. Associated Landau-Zener avoided crossings would be a source of exponentially small gaps.

Nonetheless, attempts to make this intuition exact are fraught with potential pitfalls. For increasing Γ , two randomly chosen valleys are equally likely to come either closer together or further apart in energy. In the case of the former, and further, if the sensitivity of energy levels to changes in the transverse field is so large that the levels ‘collide’ before either valley disappears, then avoided crossing will occur. This may not be necessarily the case when one considers ‘collisions’ with the ground state, which are of particular concern to QA. The ground state corresponds to a valley with the lowest energy: this and other low-lying valleys obey fundamentally different statistics of the extremes.

Case in point is the analysis of ref. 27, which develops perturbation theory in Γ . The classical limit ($\Gamma = 0$) is used as a starting point; how this analysis might be extended to $\Gamma > 0$ has also been discussed³⁰. A type of constraint satisfaction problem (CSP) has been considered: classical energy levels are discrete non-negative integers (number of violated constraints) but have exponential degeneracy. ‘Zeeman splitting’ for $\Gamma > 0$ scales as \sqrt{N} , which, for large problems, may be sufficient to overcome the $O(1)$ classical gap and cause avoided crossings of levels associated with different classical energies. Yet, this trend disappears if only levels with the smallest energies (after splitting) are considered: these are relevant for avoided crossings with the ground state. This about-face is not immediately apparent, only coming into play for $N \gtrsim 100$, when the exponential degeneracy of the classical ground state sets in. It has, however, been confirmed with analytical argument and numerics²⁹. Consequently, arguments based on perturbation theory cannot be used

to establish the transverse field chaos.

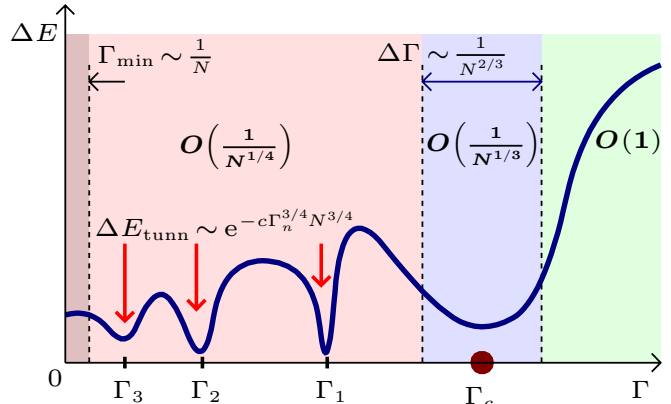


FIG. 1. Sketch of the behavior of the gap in the paramagnetic phase ($\Gamma > \Gamma_c$), the glassy phase ($\Gamma < \Gamma_c$) and the critical region ($\Gamma \approx \Gamma_c$). Scaling of the *typical* gap in these regions is indicated in bold letters using big-O notation. The area $\Gamma < \Gamma_{\min} \sim 1/N$ is where the discrete nature of the energy landscape becomes manifest: the ground state becomes nearly completely localized. The glassy phase also contains $\log N$ isolated bottlenecks, indicated with red arrows, where the gaps scales as a stretched exponential.

This manuscript offers a fresh perspective, illustrated by studying quantum annealing of Hopfield model. Mean-field analysis correctly describes thermodynamics if the number of random ‘patterns’ is small. The method is further extended to extract information about exact quantum energy levels. Importantly, classical energy landscape is made much more complex by insisting that the distribution of disorder is Gaussian. Fig. 1 sketches a ‘phase diagram’ obtained for this model. For decreasing Γ the gap changes as follows: (1) it is finite (does not scale with N) in the paramagnetic phase, $\Gamma > \Gamma_c$; (2) scales as $1/N^{1/3}$ in the paramagnetic region of width $1/N^{2/3}$ around $\Gamma = \Gamma_c$; (3) increases slightly, with typical values scaling as $1/N^{1/4}$, for $\Gamma < \Gamma_c$. In addition, there are avoided crossings at isolated points $\Gamma_1, \Gamma_2, \dots$, which is a manifestation of the transverse field chaos, demonstrated conclusively in this work.

The first non-trivial example requires two Gaussian patterns. In this case the ‘energy landscape’ is effectively one-dimensional, which greatly simplifies the analysis. The most important element of is accounting for an extreme value statistics associated with valleys (local minima) with the lowest energies. To this end, the distribution of energies of the classical landscape must be conditioned so that they are never below the energy of the global minimum. This becomes feasible when reformulated as a continuous random process, in the limit $N \rightarrow \infty$.

It emerges that the energy landscape displays fractal properties, and role of the transverse field is to approximately coarse-grain it on scales determined by Γ , eliminating small barriers: The number of valleys decreases as Γ grows. A specific random process (energy landscape

of ‘infinite’-size instance) will contain every possible realization of itself at some ‘length scale’. Some realizations will contain high barriers that cannot be easily overcome: these will lead to tunneling bottlenecks. Locations (in Γ) will depend on specific disorder realization, but due to self-similarity the successive ratios Γ_n/Γ_{n+1} should converge to a universal distribution. In a finite system, the total number will grow as

$$\mathcal{N}_{\text{tunn}} \approx \alpha \ln N. \quad (3)$$

This is far less than a power law seen in some phenomenological models of temperature chaos³¹. The slow logarithmic rise is likely a universal feature, while the prefactor is model-dependent. Its numerical value can be used to estimate the minimum problem size for which the mechanism becomes relevant, via $\mathcal{N}_{\text{tunn}} \approx 1$. A value of $\alpha \approx 0.15$ is obtained for the problem at hand, so that additional bottlenecks become an issue for $N \gtrsim 1000$. Prior numerical studies similarly require large sizes before the exponentially small minimum gap is observed²⁸, and so far there has been no evidence of two or more exponentially small gaps coexisting. The slow, logarithmic increase of the expected number of bottlenecks is the most likely culprit.

These new tunneling bottlenecks are, in some sense, related to the $\Gamma = 0$ classical fixed point: the energy gap there vanishes as $1/N$ asymptotically. The $\log N$ -behavior is a trivial consequence of universal scaling: this is how many bottlenecks can fit between $\Gamma_{\min} \sim 1/N$ determined by the minimum energy scale and $\Gamma_c \sim 1$. A notable feature of these results is that tunnelings become progressively easier as $\Gamma \rightarrow 0$ despite the fact that the model becomes more classical. Tunneling gaps increase as

$$\Delta E_{\text{tunn}}^{(n)} \sim e^{-c\Gamma_n^{3/4}N^{3/4}}. \quad (4)$$

Notice that they cease to be exponentially small for $\Gamma \lesssim \Gamma_{\min}$: at that point the ground state is already localized near the correct global minimum.

A finding that the gaps *increase* for smaller Γ deserves explanation. Typically, valleys with similar energies differ by up to $N/2$ spin flips. This changes once lowest energies are considered: all spin configurations with energies less than ϵ above the global minimum are contained in a neighborhood of radius $O[(N\epsilon)^{2/3}]$, using Hamming distance as a metric. The problem is not rendered easy by the mere fact that the global minimum is so pronounced (although specialized algorithm is efficient for $p = 2$ Hopfield network). It does imply, however, that the ground state wavefunction does not jump chaotically: Every subsequent tunneling involves shorter distances, $O(\Gamma N)$ spin flips, and achieves progressively better approximation to the true global minimum. Absent such a trend, annealing would be most difficult toward the end of the algorithm, when $\Gamma \sim 1/N$, and the minimum gap would exhibit far worse exponential scaling²⁷.

In what follows, the model and its solution are described in greater detail.

Quantum Hopfield network. Consider a model with rank- p matrix of interactions and no longitudinal field ($h_i = 0$):³²

$$J_{ik} = \frac{1}{N} \sum_{\mu=1}^p \xi_i^{(\mu)} \xi_k^{(\mu)} \quad (5)$$

(cf. $\text{rk } J_{ik} = N$ for SK model), where $\xi_i^{(\mu)}$ are taken to be i.i.d. random variables of unit variance. Thermodynamics of this quantum Hopfield model had been worked out in great detail by Nishimori and Nonomura³³. In fact, that study motivated the development of QA⁴.

When p is small ($J_{ik} \sim 1/N$), it is appropriate to replace local longitudinal fields with their mean values $h_i = \sum_k J_{ik} \langle \sigma_k^z \rangle$. The identity $\langle \sigma_i^z \rangle = h_i / \sqrt{\Gamma^2 + h_i^2}$ is used to close this system of equations. For a transverse field below the critical value, $\Gamma < \Gamma_c = 1$, there appears a non-trivial ($\mathbf{m} \neq 0$) solution to the self-consistency equation for the macroscopic order parameter, a vector with p components:

$$\mathbf{m} = \frac{1}{N} \sum_{i=1}^N \boldsymbol{\xi}_i \langle \hat{\sigma}_i^z \rangle. \quad (6)$$

Here, the disorder variables are also written using vector notation: $\boldsymbol{\xi}_i = (\xi_i^{(1)}, \dots, \xi_i^{(p)})$.

This model is equivalent to the Curie-Weiss (quantum) ferromagnet, which has a continuous phase transition characterized by a set of mean-field critical exponents. Two of these are particularly useful in the analysis of the annealing complexity: the one for the singular component of the ground state energy ($E_0^{\text{sing}}/N \propto |\gamma|^a$) as well as the dynamical exponent for the gap ($E_1 - E_0 \propto \gamma^b$), where $\gamma = \Gamma - \Gamma_c$ is the ‘distance’ from the critical point. These exponents are defined for the *infinite* system, yet fairly general heuristic analysis predicts *finite-size* scaling for the QCP bottleneck:

$$\Delta E_c \propto N^{-\frac{b}{a-b}}, \quad \Delta \Gamma_c \propto N^{-\frac{1}{a-b}}. \quad (7)$$

Substituting values $a = 2$ and $b = 1/2$ for the problem at hand one may estimate the gap at the critical point and the width of the critical region to be $O(N^{-1/3})$ and $O(N^{-2/3})$ respectively.

Worse-than-any-polynomial complexity of quantum annealing might be expected for the the first order phase transition, which exhibits no critical scaling (but see ref.³⁴ for an exception). Another possibility is for the dynamical exponent to diverge at the infinite randomness QCP: the finite-size gap scales as $\exp(-c\sqrt{N})$ in a random Ising chain²³. For the Hopfield model, however, this scaling is polynomial, as the disorder is irrelevant at the critical point. More intriguing is the fact that these pessimistic scenarios are not found in SK spin glass either: it is characterized by the same set of critical exponents, albeit with logarithmic corrections^{24–26}. These corrections to scaling increase the gap and, respectively, decrease

the width of the critical region by a factor of $\log^{2/9} N$. Thus, as long as $T_{\text{ann}} \gtrsim N$, non-adiabatic transitions at the critical point should be suppressed. This presents a conundrum as SK model is known to be an NP-hard problem: finding a polynomial-time (even in typical case) quantum algorithm would be a surprising development.

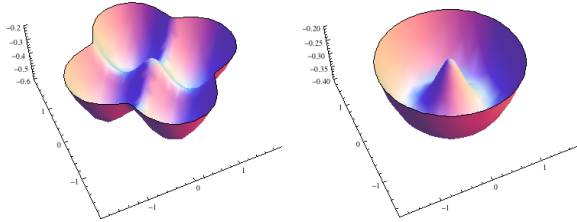


FIG. 2. The shape of the disorder-averaged effective potential $\mathcal{V}(\mathbf{m})$ for $\Gamma = 0.2 < \Gamma_c$ for the choice of bimodal (left) and Gaussian (right) distribution of disorder variables. For bimodal distribution, the $2p$ -fold degenerate global minima are organized in pockets corresponding to encoded patterns. For Gaussian distribution, the degenerate minima form a continuum, connected by arbitrary rotations.

Exact low-energy spectrum. Mean field theory can be derived in more systematic manner, via Hubbard-Stratonovich transformation. Finite-temperature partition function $Z(\beta) = \text{Tr}(e^{-\beta H})$ can be written as a path integral over $\mathbf{m}(t)$, which now acquires a dependence on the imaginary time $0 \leq t \leq \beta$, with periodic boundary conditions: $\mathbf{m}(\beta) = \mathbf{m}(0)$. The value of the integral is dominated by stationary paths corresponding to a minimum of an effective potential $\mathcal{V}(\mathbf{m})$. While the discussion above had been deliberately equivocal on the distribution of disorder variables, it is now instructive to contrast bimodal ($\xi_i^{(\mu)} = \pm 1$) and Gaussian choices. The shapes of the effective potential for both scenarios are depicted in Fig. 2.

The conventional bimodal choice defines the model of associative memory: in the limit $\Gamma = 0$ the ‘patterns’ can be perfectly recalled ($s_i = \pm \xi^{(\mu)}$) when p is small. For Gaussian choice, the global minimum corresponds to a mixture³⁵

$$s_i = \pm \text{sgn}\left(\sum_{\mu} \alpha_{\mu} \xi_i^{(\mu)}\right), \quad (8)$$

rendering memory useless. In the bimodal case, such ‘spurious’ states only become stable once the number of patterns scales with the problem size³⁶: $p > 0.05N$. The BC_p (bimodal) or $\text{O}(p)$ (Gaussian) symmetry of the effective potential is only approximate, to leading order in N . The degeneracy of the ground state is 2 (due to global spin inversion symmetry) for almost all disorder realizations when $p \geq 3$ or $p \geq 2$ in the bimodal and Gaussian scenarios respectively³⁷. The system is in a symmetric superposition of the degenerate global minima at the end of QA: it evolves entirely in the symmetric subspace since time-dependent Hamiltonian commutes with

$\hat{U} = \exp(\pi i \hat{S}^x)$. Thus, it should be noted that small gaps between symmetric and antisymmetric wavefunctions are irrelevant to QA and can be ignored.

Disorder fluctuations ‘nudge’ QA toward the ‘correct’ pattern as it passes the critical point in the bimodal Hopfield model. No further bottlenecks are encountered: gaps for $\Gamma < \Gamma_c$ as well as the ‘classical’ ($\Gamma = 0$) gap are $O(1)$. By contrast, the classical gap scales as $O(1/N)$ in the Gaussian Hopfield model, alerting to ‘danger’ posed by the $\Gamma = 0$ ‘fixed point’. To find the low-energy spectrum when $\Gamma < \Gamma_c$, note that the dominant contribution to the path integral is from paths where the magnitude of the ‘magnetization’ vector remains constant, close to its saddle-point value, while the angle is a slow function of time: $\mathbf{m}(t) \approx m_{\Gamma} \begin{pmatrix} -\sin \vartheta(t) \\ \cos \vartheta(t) \end{pmatrix}$ for $p = 2$. Integrating out the amplitude degrees of freedom, the partition function is rewritten as

$$Z(\beta) \propto \int [d\vartheta(t)] e^{-\int_0^{\beta} \left(\frac{M}{2} \left(\frac{d\vartheta}{dt}\right)^2 + V_{\Gamma}(\vartheta)\right) dt}, \quad (9)$$

which describes a quantum-mechanical particle of mass $M = O(N)$ moving on a ring, subjected to a random potential

$$V_{\Gamma}(\vartheta) = - \sum_i \sqrt{\Gamma^2 + m_{\Gamma}^2 \xi_i^2 \sin^2(\vartheta - \theta_i)} + N \langle \sqrt{\dots} \rangle_{\xi}, \quad (10)$$

where $\xi_i \equiv \xi_i \begin{pmatrix} \cos \theta_i \\ \sin \theta_i \end{pmatrix}$ and the last term, written in shorthand, adds a constant offset so that $\langle V(\vartheta) \rangle_{\xi} = 0$. Notice that $V_{\Gamma}(\vartheta) \propto \sqrt{N}$ via central limit theorem, representing a higher-order correction to the extensive part of the free energy.

Since the partition function $Z(\beta) = \sum_n e^{-\beta E_n}$ encodes information about the spectrum, low-energy (Goldstone) excitations of the many-body problem are in one-to-one correspondence with the energy levels of a quantum mechanical particle, up to a constant shift.

Evolution of the random potential. Scaling of the gap for $\Gamma < \Gamma_c$ can be obtained via semiclassical analysis. Small level splitting due to tunneling between wells at two degenerate global minima ($V_{\Gamma}(\vartheta + \pi) = V_{\Gamma}(\vartheta)$ as a consequence of global Z_2 symmetry) is not relevant to QA. Higher degeneracies are statistically unlikely; quantization rules predict $O(N^{-1/4})$ gaps between energy levels with the symmetric subspace. But this refers to the *typical* gap, obtained for *fixed* Γ for *almost all* realizations of disorder. As quantum annealing *sweeps* the transverse field for a *fixed* realization of disorder, $V_{\Gamma}(\vartheta)$ might undergo global bifurcation. This would result in a small tunneling gap for a specific value of Γ when the competing minima are in resonance.

Such a scenario is impossible near the QCP: Coefficients in the Fourier expansion of the random potential, $\sum_k (a_k \cos 2k\vartheta + b_k \sin 2k\vartheta)$ decrease as m^{2k}/Γ^{2k-1} so that the first harmonic dominates for $\Gamma \approx \Gamma_c$. Semiclassical analysis confirms $O(N^{-1/3})$ gap at the critical

point (where the curvature of the effective potential vanishes, leaving only the quartic part). As Γ decreases, the random potential becomes more rugged, smooth only on scales $\Delta\vartheta \sim \Gamma$, which makes global bifurcations more likely. Furthermore, it exhibits properties that allow one to make important predictions without detailed calculations: Rescaling the potential in the vicinity of either global minimum $V_\Gamma(\vartheta^*) = V_\Gamma^*$,

$$\begin{aligned} \vartheta - \vartheta^* &\rightarrow \ell(\vartheta - \vartheta^*), \\ V_\Gamma - V_\Gamma^* &\rightarrow \ell^{3/2}(V_\Gamma - V_\Gamma^*), \end{aligned} \quad (11)$$

describes the same model, but for the rescaled $\Gamma \rightarrow \ell\Gamma$ and a different realization of disorder. This invariance implies that *if global bifurcations do occur*, their density ought to be uniform in $\log \Gamma$. It follows that the number of such bottlenecks would be $O(\log N)$, using natural cutoffs at $\Gamma_{\min} \sim 1/N$ (corresponding to the minimum energy scale) and $\Gamma_{\max} \sim 1$ (QCP). Yet, to guarantee that the density of bifurcations is non-zero, it becomes necessary to examine the properties of the random potential in the classical limit $\Gamma = 0$.

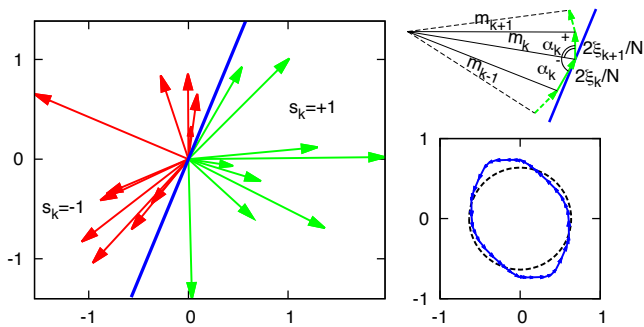


FIG. 3. Geometric interpretation of the random potential, illustrated for a random instance with $N = 20$. Vector $\mathbf{m}(\vartheta)$ is defined by drawing a separating line at angle ϑ and assigning spins with ξ_i on either side of separating line values $s_i = +1$ and $s_i = -1$ respectively (left figure). For changing ϑ vector $\mathbf{m}(\vartheta)$ is incremented/decremented by $(2/N)\xi_i$ (top right). The increments form a closed path, approximated by a circle; fluctuations define a random potential (bottom right).

The classical optimization problem corresponds to maximizing the magnitude of $\sum_i \xi_i s_i$. A necessary condition for a local minimum is that two sets of vectors — $\{\xi_i | s_i = +1\}$ and $\{\xi_i | s_i = -1\}$ — can be separated by a line. As the angle of this line changes, fluctuations of the amplitude give rise to a random potential $V_0(\vartheta)$ (see Fig. 3). This suggests a linear-time algorithm for finding a global minimum³⁸, but quantum annealing algorithm is too generic to exploit a specific structure of the problem.

On short intervals, the random process is described as undamped Langevin process^{39,40} in the continuous ($N \rightarrow \infty$) limit (hence the exponent of 3/2 in eqn. (11), corresponding to its fractal dimension). Properly taking into account the statistics of the extremal properties, the process must be conditioned on the fact that

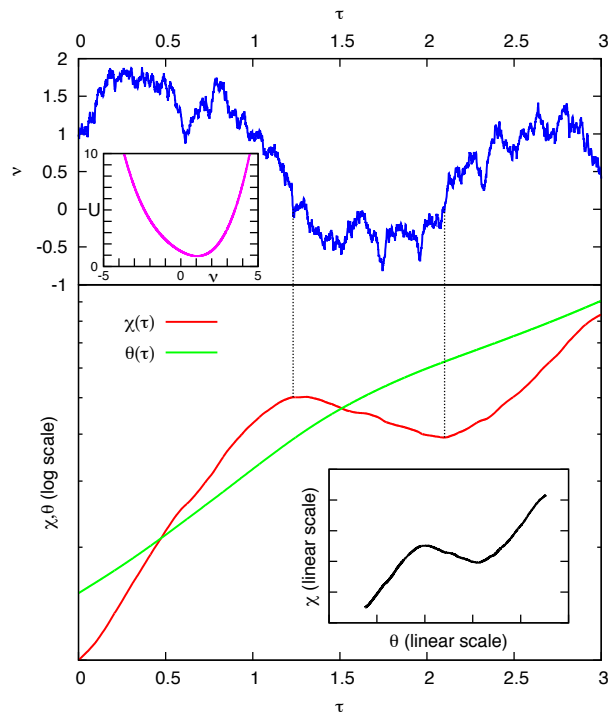


FIG. 4. Illustration of appearance of local minima. Top figure plots the Langevin potential $\mathcal{U}(\nu)$ (inset) and a particular realization of stochastic process $\nu(\tau)$. It is integrated twice to produce $\chi(\tau)$ and $\vartheta(\tau)$ in the lower figure. Lower inset plots χ as a function of ϑ . Regions with $\nu(\tau) < 0$ are responsible for the appearance of local minima.

$V_0(\vartheta) > V_0(\vartheta_0^*) = V_0^*$ away from the global minimum. As described in Methods and the Supplement, such a conditioned process consists of two uncorrelated branches, $V_0(\vartheta) - V_0^* \propto \sqrt{N} \begin{cases} \chi_+, & \vartheta > \vartheta_0^* \\ \chi_-, & \vartheta < \vartheta_0^* \end{cases}$. Integrating equations

$$\begin{aligned} d(\ln \chi_\pm)/d\tau &= \nu_\pm(\tau), \\ d\vartheta/d\tau &= \pm \chi_\pm^{2/3}, \end{aligned} \quad (12)$$

defines $\chi_+(\vartheta)$ and $\chi_-(\vartheta)$ parametrically, in terms of random processes $\nu_\pm(\tau)$ corresponding to the Brownian motion in a non-linear potential depicted in Fig. 4. This potential is biased toward positive ‘velocities’ ν so that $V_0 - V_0^* \sim \sqrt{N}(\vartheta - \vartheta_0^*)^{3/2}$ from eqn. (12). It will, however, experience arbitrary percentage drops due to subpaths with $\nu < 0$ (albeit with decreasing probability).

For small but finite Γ , the ‘separating line’ becomes blurred. The random potential adds a ‘quantum correction’ (see Methods and the Supplement), $V_\Gamma(\vartheta) - V_0(\vartheta) = O(\sqrt{N}\Gamma^{3/2})$. For two minima to come into resonance, they cannot be more than $\Delta\vartheta \sim \Gamma$ apart (i.e. $O(N\Gamma)$ spin flips). The tunneling exponent is given by under-the-barrier action $\mathcal{A} \sim \sqrt{M\Delta V\Delta\vartheta}$, where the effective mass $M \sim N/\Gamma^2$ and $\Delta V \sim \sqrt{N}\Gamma^{3/2}$. Numerical results for the universal distribution of tunneling jumps and the tunneling exponents are exhibited in Fig. 5.

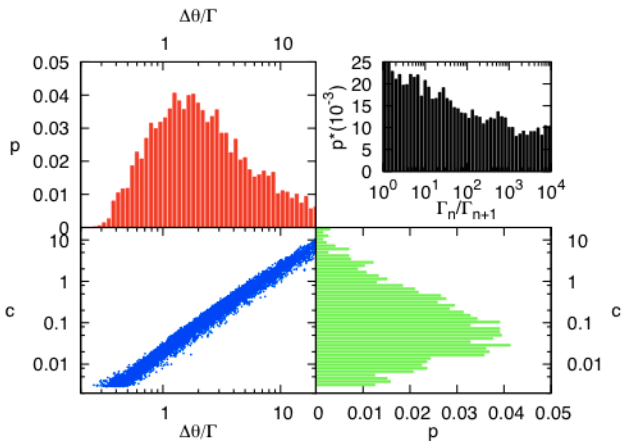


FIG. 5. Numerical results. L-shaped figure plots the distribution of tunneling jumps and exponent. Lower left quadrant is a scatterplot of $\Delta\theta/\Gamma$ (proportional to the number of spin flips normalized by ΓN) against $|\log \Delta E_{\text{tunn}}|/(\Gamma N)^{3/4}$ (the prefactor c) for all tunneling events. Histograms of these quantities alone (projections of the scatterplot) are in the top left and bottom right quadrants. Top right figure plots a histogram of distribution of Γ_n/Γ_{n+1} for successive tunneling events.

Concluding remarks. Using a simple model, this manuscript successfully demonstrates a phenomenon of transverse field chaos and its implications for the performance of quantum adiabatic annealing. This is particularly impactful for a model of mean-field spin glass, where the existence of temperature chaos⁴¹ — a classical counterpart — had been debated^{42–44}. Ref.⁴³ in particular reports an extremely weak effect in SK model, appearing in 9th order of perturbation theory expansion. By contrast, temperature chaos in Edwards-Anderson spin glass is uncontroversial^{45,46}.

To dwell upon the generality of these results, first note that scaling of the tunneling exponent will depend on the universality class of the model. SK model, for instance, exhibits different scaling of barrier heights, believed to be $\propto N^{1/3}$ (see e.g. ref. 47). In the model studied, the decrease in the number of spins involved in tunnelings offsets the divergence of the effective mass in the classical limit $\Gamma \rightarrow 0$. As the height of the barriers also decreases, the tunneling gaps widen toward the end of the algorithm. One might expect qualitatively similar behavior in realistic spin glasses.

The logarithmic scaling of the number of bottlenecks is due to self-similar properties of free energy landscape in the interval $[\Gamma_{\min}, \Gamma_c]$. The lower cutoff should correspond to the smallest energy scale in the classical limit, which for SK model is also a negative power of N . The scaling of the classical gap is $1/\sqrt{N}$, due to spins subjected to very small effective fields at zero temperature (the density of distribution of effective fields vanishes linearly as $h \rightarrow 0$, see ref. 48). The picture is less clear for

constraint satisfaction problems, where the energies are constrained to be non-negative integers; i.e. the classical gap is $O(1)$. Avoided crossings disappear in the Hopfield model with a small number of patterns drawn from a bimodal distribution. That, however, could be due to the fact that the number of valleys is also small. More typically, energy levels in CSPs have exponential degeneracy, which is lifted by the transverse field. A value sufficient to make the spectrum effectively quasi-continuous might serve as an appropriate lower cutoff Γ_{\min} in problems of this type.

METHODS

Finite-size scaling of the gap at QCP is best understood using an example of a finite-dimensional system. In thermodynamic limit, both correlation length and the characteristic time diverge near the phase transition as

$$\xi_c \propto (\Gamma - \Gamma_c)^{-\nu}, \quad \tau_c \propto (\Gamma - \Gamma_c)^{-z\nu}. \quad (13)$$

In a finite system this divergence is smoothed out as soon as the correlation length becomes comparable to lattice size ($\xi_c \sim N^{1/d}$). The minimum gap (the reciprocal of τ) and the width of the critical region should scale as $N^{-z/d}$ and $N^{-1/(d\nu)}$ respectively. In this paper, the product $z\nu$ has been labeled as exponent b . Singular behavior of normalized ground state energy (free energy) is related to the specific heat exponent ($a = 2 - \alpha$). Dimensionality d can be eliminated with the aid of hyperscaling relation $2 - \alpha = (d + z)\nu$ to yield eqn. (7) of the main text. Independent estimates of the specific heat exponent can be obtained from the exponents for the order parameter and the susceptibility ($2 - \alpha = 2\beta + \gamma$).

Finite-temperature partition function can be written as a sum over a set of paths $\{s_i(t)\}$ with $0 \leq t \leq \beta$, where $s_i(t)$ alternates between the values ± 1 . Hubbard-Stratonovich transformation can be used to rewrite it as a path integral

$$\begin{aligned} Z &\sim \sum_{\{\{s_i(t)\}\}} e^{\frac{1}{2N} \int_0^\beta (\sum_i \xi_i s_i(t))^2 dt + \sum_i \mathcal{K}_\Gamma[s_i(t)]} \\ &\sim \int [d\mathbf{m}(t)] e^{-\frac{N}{2} \int_0^\beta \mathbf{m}^2(t) dt + \sum_i \ln Z_i}. \end{aligned} \quad (14)$$

The ‘kinetic’ term $\mathcal{K}_\Gamma[s(t)]$ in the first equation penalizes kinks, representing Γ -dependent ferromagnetic couplings between Trotter slices. As the interaction term is decoupled, the problem reduces to that of evaluating the single-site partition function Z_i for a spin subjected to a magnetic field with the transverse component Γ and the ‘time-dependent’ longitudinal component $h_i(t) = \xi_i \mathbf{m}(t)$. To leading order in N , the saddle-point of the path integral (14) is a solution of mean field equations. This becomes a degenerate manifold for Gaussian disorder distribution; to determine higher-order contribution all paths such that $|\mathbf{m}(t)| = m_\Gamma$ are considered. Evaluating Z_i is best performed in the adiabatic basis that diagonalizes the 2-level Hamiltonian $\hat{H}_i = -h_i(t)\hat{\sigma}^z - \Gamma\hat{\sigma}^x$,

$$Z_i = \text{Tr} \mathcal{T} e^{\int_0^\beta H_i(t) dt} = \text{Tr} \mathcal{T} e^{-\int_0^\beta (\hat{E}_i(t) + i \frac{\partial}{\partial t} \hat{V}_i(t)) dt}. \quad (15)$$

Here $\hat{E}_i(t)$ is diagonal with eigenvalues $\pm \sqrt{\Gamma^2 + h_i^2(t)}$. Its fluctuations around the mean give rise to the random potential $V_\Gamma(\vartheta)$. Non-adiabatic terms due to rotation of the basis ($\hat{U} = e^{i\hat{V}_i(t)}$) are treated using 2nd order perturbation theory, giving rise to a kinetic term $\propto (d\vartheta/dt)^2$.

In the limit $N \rightarrow \infty$, the random potential $V_\Gamma(\vartheta)$ defined in eqn. (10) in the main text converges to a Gaussian process that can be specified completely by its covariance matrix $\langle V_\Gamma(\vartheta) V_{\Gamma'}(\vartheta') \rangle$. This can be ‘diagonalized’, alternatively expressing the random potential as a linear combination of white-noise processes $\{\zeta_n(\vartheta)\}$.

One representation, as a convolution series $\sum_{n=0}^{\infty} (f_{\Gamma}^{(n)} \star \zeta_n)(\vartheta)$ with kernels

$$f_{\Gamma}^{(n)}(\vartheta) \propto \int_0^{\infty} \sqrt{\Gamma^2 + \xi^2 m_{\Gamma}^2 \sin^2 \vartheta} \xi^{\alpha+1} e^{-\xi^2/2} L_n^{(\alpha)}\left(\frac{\xi^2}{2}\right) d\xi, \quad (16)$$

relies on orthogonal properties of associated Laguerre polynomials. The choice $\alpha = 1$ ensures that only $n = 0$ term survives in the limit $\Gamma = 0$. The random potential should satisfy a stochastic equation

$$\frac{d^2 V_0}{d\vartheta^2} + V_0 = \frac{2\sqrt{N}}{\pi} \zeta_0. \quad (17)$$

As a side note observe that similar equation is obtained by taking a continuous limit in the identities that follow from elementary geometry (see Fig. 3 in the main text, $V_k = \frac{N}{2} m_k^2$):

$$\frac{V_{k+1} - V_k}{\xi_{k+1}} - \frac{V_k - V_{k-1}}{\xi_k} = \frac{2}{N} (\xi_{k+1} + \xi_k) + 4\sqrt{2V_k/N} \cos \frac{\alpha_k^+ - \alpha_k^-}{2} \cos \frac{\alpha_k^+ + \alpha_k^-}{2} \quad (18)$$

For finite Γ , the form of the potential is modified as follows: It is convolved with a smoothing kernel of width $\Delta\vartheta \sim \Gamma$, which raises the global minimum by $O(\sqrt{N}\Gamma^{3/2})$. Additional random contributions (from $n \geq 1$) have similar scaling.

In the vicinity of the global minimum, the statistics of the classical potential is fundamentally different. The ‘returning force’ in eqn. (17) can be neglected; additionally the process should be conditioned on the fact that it stays above its value at $\vartheta = 0$ (no generality is lost by choosing the global minimum as the origin). This problem has been a subject of considerable body of work^{39,40}, although important aspects ought to be revisited. Here, I present a particularly simple self-contained derivation.

A pair (χ, v) — where $\chi \propto V_0 - V_0^*$ is interpreted as the ‘coordinate’ and $v = d\chi/d\vartheta$ as the ‘velocity’ (ϑ being ‘time’) — forms a Markov process. The probability distribution $p(\vartheta; \chi, v)$ satisfies, for $\vartheta > 0$,

$$\frac{\partial p}{\partial \vartheta} = -v \frac{\partial p}{\partial \chi} + \frac{1}{2} \frac{\partial^2 p}{\partial v^2}, \quad \text{while } p(\vartheta; +0, v) = 0 \quad (\forall v > 0) \quad (19)$$

serves as a boundary condition for the absorbing boundary. This probability is ‘renormalized’ to condition on the fact that it survives until some $\Theta \gg \vartheta$. It becomes a conserved quantity, but the diffusion equation adds a drift, $-\partial(\log P_{\Theta})/\partial v$, repelling from the boundary. The ‘survival’ probability P_{Θ} in the limit $\Theta \rightarrow \infty$ is, up to ‘time-reversal’, the universal asymptotic solution of (19), reduced to ordinary differential equation (ODE) using scaling ansatz:

$$p(\vartheta, \chi, v) \propto \frac{\chi^{2\alpha/3} p_*(v/\chi^{1/3})}{\vartheta^{\alpha}}. \quad (20)$$

This exploits a fact that fractal dimensions of ‘velocity’ and ‘coordinate’ are $[v] = [\vartheta]^{1/2}$ and $[\chi] = [\vartheta]^{3/2}$. Asymptotics is dominated by solutions with the smallest possible exponent, $\alpha = 1/4$ out of the infinite set of eigenvalues for the ODE. This matches a known value obtained with a different method³⁹.

The next step performs a change of variables, introducing ‘dimensionless’ velocity $\nu = v/\chi^{1/3}$, and ‘logarithmic’ coordinate $\mu = \ln \chi$. With the ‘time’ variable redefined via $d\tau = d\vartheta/\chi^{2/3}$, Markov process is described by a *triple* (ϑ, μ, ν) . Marginalizing out μ and ϑ in the equation for $p(\tau; \vartheta, \mu, \nu)$ produces Fokker-Planck equation for a stochastic motion of particle in a potential

$$\mathcal{U}(\nu) = -\ln \left((\nu/6^{1/3}) \text{Ai}(\nu^2/6^{2/3}) + \text{Ai}'(\nu^2/6^{2/3}) \right) \quad (21)$$

Given a particular realization of $\nu(\tau)$, full process (μ, ν, ϑ) is determined deterministically, by integration (see eqn. (12) in the main text). The construction of a realization of random process is performed independently for $\vartheta > 0$ and $\vartheta < 0$.

Numerical simulations rescale this random potential instead of evolving the transverse field: $\vartheta \mapsto e^{-\frac{\Delta\Gamma}{\Gamma}} \vartheta$ and $\chi \mapsto e^{-\frac{3}{2} \frac{\Delta\Gamma}{\Gamma}} \chi$. The process is extended to larger values of τ as needed (details of the process for small τ , where they fall below the numerical precision, are ‘forgotten’). A fairly large range of τ is required to gather the sufficient statistics.

* Sergey.I.Knysh@nasa.gov

1. Nielsen, M. & Chuang, I. *Quantum Computation and Quantum Information*, Cambridge University Press, Cambridge, MA, 10th ed. (2011).
2. Shor, P. W. Polynomial-time algorithms for prime factorization and discrete logarithms of a quantum computer. *SIAM J. Sci. Stat. Comp.* **26**, 1484 (1997).
3. Garey M. R. & Johnson D. S. *Computers and Intractability: A Guide to the Theory of NP-Completeness*. W. H. Freeman, New York, NY (1979).
4. Kadowaki, T. & Nishimori, H. Quantum Annealing in the Transverse Ising Model. *Phys. Rev. E* **58**, 5355 (1998).
5. Farhi, E., Goldstone, J., Gutmann, S., & Sipser M. Quantum Computation by Adiabatic Evolution. e-print arXiv:quant-ph/0001106.
6. Das, A. & Chakrabarti, B. K. Quantum annealing and analog quantum computation. *Rev. Mod. Phys.* **80**, 1061 (2008).
7. van Dam, W., Mosca, M. & Vazirani, U. How powerful is adiabatic quantum computation? *Proc. 42nd IEEE Symp. FOCS*, 279 (2001).
8. Brooke, J., Bitko, D., Rosenbaum, F.T. & Aeppli, G. Quantum annealing of a disordered magnet. *Science* **284**, 779–781 (1999).
9. Santoro, G., Martoňák, R., Tosatti, E. & Car, R. Theory of quantum annealing of spin glasses. *Science* **295**, 2427–2430 (2002).
10. Edwards, S. F. & Anderson, P. W. Theory of spin glasses. *J. Phys. F: Met. Phys.* **5**, 965 (1975).
11. Heim, B., Rønnow, T. F., Isakov, S. V. & Troyer, M. Quantum versus classical annealing of Ising spin glasses.
12. Farhi, E., Goldstone, J., Gutmann, S., Lapan, J., Lundgren, A. & Preda, D. A quantum adiabatic evolution algorithm applied to random instances of an NP-complete problem. *Science* **292**, 472–475 (2001).
13. Young, A. P., Knysh, S., & Smelyanskiy, V. N. First order phase transition in the quantum adiabatic algorithm. *Phys. Rev. Lett* **104**, 020502 (2010).
14. Boixo, S. *et al.* Evidence for quantum annealing with more than one hundred qubits. *Nat. Phys.* **10**, 218–224 (2014).
15. Rønnow, T. F. *et al.* Defining and detecting quantum speedup. *Science* **345**, 420–424 (2014).
16. Boixo, S. *et al.* Computational role of multiqubit tunneling in a quantum annealer. e-print arXiv:1502.05754 (2015).
17. Katzgraber, H. G., Hamze, F., Zhu, Z., Ochoa, A. J. & Munos-Bauza, H. Seeking Quantum Speedup through Spin Glasses: The Good, the Bad, and the Ugly. e-print arXiv:1505.01545 (2015).
18. Zhu, Z., Ochoa, A. J., Schnabel, S., Hamze, F. & Katz-

- graber, H. G. Best-case performance of quantum annealers on native spin-glass benchmarks: How chaos can affect success probabilities. e-print arXiv:1505.02278 (2015).
19. Smelyanskiy, V. N., von Toussaint, U. & Timucin, D. A. Dynamics of quantum adiabatic evolution algorithm for number partitioning. e-print arXiv:quant-ph/0202155 (2002).
 20. Goldschmidt, Y. Y. *Phys. Rev. B* **41**, 4858(R) (1990).
 21. Jörg, T., Krzakała, F., Kurchan, J. & Maggs, A. C. Simple glass models and their quantum annealing. *Phys. Rev. Lett.* **101**, 147204 (2008).
 22. Jörg, T., Krzakała, F., Semerjian, G. & Zamponi, F. First-order transitions and the performance of quantum algorithms in random optimization problems. *Phys. Rev. Lett.* **104**, 207206 (2010).
 23. Fisher, D. S. Critical behavior of random transverse-field Ising spin chains. *Phys. Rev. B* **51**, 6411 (1995).
 24. Miller, J. & Huse, D. Zero-temperature critical behavior of the infinite-range quantum Ising spin glass. *Phys. Rev. Lett.* **70**, 3147 (1993).
 25. Ye, J., Sachdev, S. & Read, N. Solvable spin glass of quantum rotors. *Phys. Rev. Lett.* **70**, 4011 (1993).
 26. Read, N., Sachdev, S. & Ye, J. Landau theory of quantum spin glasses of rotors and Ising spins. *Phys. Rev. B* **52**, 384 (1995).
 27. Altshuler, B., Krovi, H. & Roland, J. Anderson localization casts clouds over adiabatic quantum optimization, *Proc. Nat. Acad. Sci. USA* **107**, 12446–12450 (2010).
 28. Farhi, E., Gosset, D., Hen, I., Sandvik, A. W., Shor, P., Young, A. P. & Zamponi, F. The performance of the quantum adiabatic algorithm on random instances of two optimization problems on regular hypergraphs. *Phys. Rev. A* **86**, 052334 (2012).
 29. Knyslysh, S. & Smelyanskiy, V. N. On the relevance of avoided crossings away from quantum critical point to the complexity of quantum adiabatic algorithm. e-print arXiv:1005.3011 (2010).
 30. Laumann, C. R., Moessner, R., Scardicchio, A. & Sondhi, S. L. Quantum annealing: the fastest route to quantum computation? *Eur. Phys. J. ST* **224**, 75–88 (2015).
 31. Krzakała, F. & Martin, O. C. Chaotic temperature dependence in a model of spin glasses. *Eur. Phys. J. B* **28**, 199–209 (2002).
 32. Hopfield, J. Neural networks and physical systems with emergent collective computational abilities. *Proc. Nat. Acad. Sci.* **79**, 2554–2558 (1982).
 33. Nishimori, H. & Nonomura, Y. Quantum Effects in Neural Networks. *J. Phys. Soc. Japan* **65**, 3780–3796 (1996).
 34. Laumann, C. R., Moessner, R., Scardicchio, A. & Sondhi, S. L. The quantum adiabatic algorithm and scaling of gaps at first order quantum phase transitions. *Phys. Rev. Lett.* **109**, 030502 (2012).
 35. Bovier, A., van Enter, A. C. D. & Niederhauser, B. Stochastic symmetry-breaking in a gaussian Hopfield model. *J. Stat. Phys.* **95**, 181 (1999).
 36. Hertz, J., Krogh, A. & Palmer, R. G. *Introduction to the Theory of Neural Computation*, Addison-Wesley, Boston, MA (1995).
 37. The $p = 2$ bimodal case possesses an additional symmetry, making the ground state 4-fold degenerate.
 38. The overhead of sorting may introduce an extra $\log N$ factor.
 39. Sinai, Y. G. On the distribution of some functions of the integral of a random walk. *Teor. Mat. Fiz.* **90**, 323 (1992).
 40. Groeneboom, P., Jongbloed, G. & Wellner, J. A. Integrated brownian motion, conditioned to be positive. *Ann. Prob.* **27**, 1283–1303 (1999).
 41. Bray, A. J. & Moore, M. A. Chaotic nature of the spin-glass phase. *Phys. Rev. Lett.* **58**, 57 (1987).
 42. Mulet, R., Pagnani, A. & Parisi, G. Against temperature chaos in naive Thouless-Anderson-Palmer equations. *Phys. Rev. B* **63**, 184438 (2001).
 43. Rizzo, T. & Crisanti, A. Chaos in temperature in the Sherrington-Kirkpatrick model. *Phys. Rev. Lett.* **90**, 137201 (2003).
 44. Billoire, A. Rare events analysis of temperature chaos in the Sherrington-Kirkpatrick model. *J. Stat. Mech.* P040016 (2014).
 45. Kondor, I. On chaos in spin glasses. *J. Phys. A* **22** L163 (1989).
 46. Katzgraber, H. G. & Krzakała, F. Temperature and Disorder Chaos in Three-Dimensional Ising Spin Glasses. *Phys. Rev. Lett.* **98**, 017201 (2007).
 47. Vertechi, D. & Virasoro, M.A., Energy barriers in SK spin-glass model. *J. Phys. France* **50**, 2325–2332 (1989).
 48. Sommers, H. J. & Dupont, W. Distribution of frozen fields in the mean-field theory of spin glasses. *J. Phys.* **C17** 5785 (1984).

ACKNOWLEDGEMENTS

I would like to thank Vadim Smelyanskiy for useful discussions. This work was supported in part by the Office of the Director of National Intelligence (ODNI), Intelligence Advanced Research Projects Activity (IARPA), via IAA 145483, and by the Air Force Research Laboratory (AFRL) Information Directorate under grant F4HBKC4162G001. The views and conclusions contained herein are those of the author and should not be interpreted as necessarily representing the official policies or endorsements, either expressed or implied, of ODNI, IARPA, AFRL, or the U.S. Government. The U.S. Government is authorized to reproduce and distribute reprints for Governmental purpose notwithstanding any copyright annotation thereon.

SUPPLEMENTARY INFORMATION

Mathematical Preliminaries. This paper makes extensive use of Meijer G-function defined via integral

$$G_{p,q}^{m,n} \left(z \left| \begin{matrix} a_1, \dots, a_n; a_{n+1}, \dots, a_p \\ b_1, \dots, b_m; b_{m+1}, \dots, b_q \end{matrix} \right. \right) = \frac{1}{2\pi i} \int_{\mathcal{L}} \frac{\prod_{k=1}^m \Gamma(b_k + s) \prod_{k=1}^n \Gamma(1 - a_k - s)}{\prod_{k=n+1}^p \Gamma(a_k + s) \prod_{k=m+1}^q \Gamma(1 - b_k - s)} z^{-s} dz, \quad (\text{S1})$$

where the contour \mathcal{L} is chosen appropriately. Bold $\Gamma(x)$ is used to denote Γ -function to avoid confusion with the transverse field variable. G-function can be used to express many elementary and special functions; those used here include:

- $e^{-x} = G_{0,1}^{1,0}(x | \bar{0})$,
- $(1+x)^{-a} = \frac{1}{\Gamma(a)} G_{1,1}^{1,1}(x | \bar{0}^{-a})$,
- $L_n^{(\alpha)}(x) e^{-x} = \frac{1}{n!} G_{1,2}^{1,1}(x | \bar{0; -\alpha}^{-n-\alpha})$,
- $U(a, b, x) = \frac{1}{\Gamma(a)\Gamma(a-b+1)} G_{1,2}^{2,1}(x | \bar{0, 1-b}^{1-a})$,

where $L_n^{(\alpha)}(x)$ are associated Laguerre polynomials and $U(a, b, x)$ represents confluent hypergeometric (Kummer) function. Multiplication by a finite power x^α merely shifts all parameters $a_1, \dots, a_n, b_1, \dots, b_m$ by constant α . Most integrals encountered can be recast as those of Mellin type:

$$\int_0^\infty G_{p,q}^{m,n} \left(\frac{x}{t} \left| \begin{matrix} \vec{a} \\ \vec{b} \end{matrix} \right. \right) G_{r,s}^{k,\ell} \left(t \left| \begin{matrix} \vec{c} \\ \vec{d} \end{matrix} \right. \right) \frac{dt}{t} = G_{p+r, q+s}^{m+k, n+\ell} \left(x \left| \begin{matrix} \vec{a}, \vec{c} \\ \vec{b}, \vec{d} \end{matrix} \right. \right), \quad (\text{S2})$$

where vectors are concatenated as follows: \vec{a}, \vec{c} consists of a_1, \dots, a_n and c_1, \dots, c_ℓ followed by a_{n+1}, \dots, a_p and $c_{\ell+1}, \dots, c_r$ (similarly for \vec{b} and \vec{d}). This ensures that zeros and poles in the Mellin transform of G-functions are grouped together.

Mean Field Analysis. Self-consistency equation for the ‘magnetization’ vector defined in eqn. (6) of the main text can be written as follows:

$$\mathbf{m} = \frac{1}{N} \sum_i \boldsymbol{\xi}_i \langle \sigma_i^z \rangle = \frac{1}{N} \sum_i \frac{\boldsymbol{\xi}_i(\boldsymbol{\xi}_i \mathbf{m})}{\sqrt{\Gamma^2 + (\boldsymbol{\xi}_i \mathbf{m})^2}}, \quad (\text{S3})$$

where the individual spins polarize along the magnetic field with the components Γ and $h_i = \boldsymbol{\xi}_i \mathbf{m}$ in the transverse and longitudinal directions respectively. Replacing sum over spins with disorder average, one obtains non-trivial solution to self-consistency equations for $\Gamma < 1$. For the bimodal distribution, the solutions are $(\pm\sqrt{1-\Gamma^2}, 0, \dots, 0)$, $(0, \pm\sqrt{1-\Gamma^2}, \dots, 0)$, etc. Other spurious solutions appear for smaller Γ , but they do not become stable for finite p . For Gaussian distribution, the magnetization vector can have arbitrary direction while the magnitude m_Γ satisfies

$$1 = \int \frac{\xi^2}{\sqrt{\Gamma^2 + \xi^2 m_\Gamma^2}} \frac{1}{\sqrt{2\pi}} e^{-\xi^2/2} d\xi = \frac{1}{\sqrt{2} m_\Gamma} U\left(\frac{1}{2}, 0, \frac{\Gamma^2}{2m_\Gamma^2}\right), \quad (\text{S4})$$

where the integral on the right hand side had been converted to Mellin type, $\int_0^\infty G_{1,1}^{1,1}(x | \bar{1/2}) G_{0,1}^{1,0}(t | \bar{1}) \frac{dt}{t}$ by substituting $t = \xi^2/2$ and $x = \Gamma^2/(2m_\Gamma^2)$. Alternatively, it can be expressed in terms of modified Bessel functions.

Low-energy spectrum of Hopfield model can be obtained by examining the partition function at finite temperature. It can be written as a sum over paths $\{s_i(t)\}$ alternating between values $s_i(t) = \pm 1$ with periodic boundary conditions $s_i(\beta) = s_i(0)$:

$$Z \sim \sum_{\{s_i(t)\}} e^{\frac{1}{2} \int_0^\beta J_{ik} s_i(t) s_k(t) dt + \sum_i \mathcal{K}_\Gamma[s_i(t)]}. \quad (\text{S5})$$

The ‘kinetic’ term $\mathcal{K}[s(t)] = (\# \text{ of kinks}) \times \frac{1}{2} \ln \coth \Gamma \Delta t$, where Δt is the discretization chosen (limit $\Delta t \rightarrow 0$ will be taken eventually). This term completely suppresses the dynamics in the limit $\Gamma = 0$.

With $J_{ik} = (1/N) \sum_\mu \xi_i^{(\mu)} \xi_k^{(\mu)}$, two-body interactions are decoupled via Hubbard-Stratonovich transformation: Using the identity $e^{\frac{1}{2N} (\sum_i \xi_i s_i)} \propto \int d\mathbf{m} e^{-\frac{N}{2} \mathbf{m}^2 + \sum_i \xi_i \mathbf{m} s_i}$, the partition function is recast as a path integral,

$$Z \sim \int [d\mathbf{m}(t)] e^{-\frac{N}{2} \int_0^\beta \mathbf{m}^2(t) dt + \sum_i \ln Z_i}, \quad (\text{S6})$$

where

$$Z_i = \sum_{[s(t)]} e^{\int_0^\beta h_i(t) s_i(t) dt + \mathcal{K}_\Gamma[s(t)]} = \text{Tr} \mathcal{T} e^{-\int_0^\beta \hat{H}_i(t) dt} \quad (\text{S7})$$

is a single-site partition function for a spin in a ‘time-dependent’ longitudinal field $h_i(t) = \boldsymbol{\xi}_i \mathbf{m}(t)$. It has been rewritten with the aid of time-ordering operator \mathcal{T} . The single-site Hamiltonian $\hat{H}_i(t) = -h_i(t) \hat{\sigma}^z - \Gamma \hat{\sigma}^x$.

The dominant contribution to the path integral is given by stationary paths, $\mathbf{m}(t) \equiv \mathbf{m}$. To leading order In this case $Z \sim \int d\mathbf{m} e^{-N\beta \mathcal{V}(\mathbf{m})}$, where the effective potential is

$$\mathcal{V}(\mathbf{m}) = \frac{\mathbf{m}^2}{2} - \left\langle \sqrt{\Gamma^2 + (\boldsymbol{\xi} \mathbf{m})^2} \right\rangle_{\boldsymbol{\xi}} = \frac{\mathbf{m}^2}{2} - \sqrt{2} |\mathbf{m}| U\left(-\frac{1}{2}; 0; \frac{\Gamma^2}{2\mathbf{m}^2}\right). \quad (\text{S8})$$

The saddle-point value $m_\Gamma = |\mathbf{m}|$ that minimizes the potential for $\Gamma = 0$ is given by a solution of eqn. (S4).

Considering higher-order corrections, the dominant contribution comes from paths where the magnitude of magnetization fluctuates around the mean field value and the angle is a slow function of time: $\mathbf{m}(t) \approx m_\Gamma \begin{pmatrix} -\sin \vartheta(t) \\ \cos \vartheta(t) \end{pmatrix}$. Since the local field $h_i(t)$ is slow-varying, it is convenient to evaluate the partition function (S7) in the adiabatic basis that diagonalizes the instantaneous 2-level Hamiltonian: $\hat{H}_i(t) = e^{i\hat{V}_i(t)} \hat{E}_i(t) e^{-i\hat{V}_i(t)}$ where

$$\hat{E}_i(t) = -\sqrt{\Gamma^2 + h_i^2(t)} \hat{\sigma}^z \text{ and } \hat{V}_i(t) = \frac{1}{2} \text{arccot} \frac{h_i(t)}{\Gamma} \hat{\sigma}^y. \quad (\text{S9})$$

Using this factorization, the time-ordered product $\text{Tr}(\dots e^{i\hat{V}_i(t+\Delta t)} e^{-E_i(t+\Delta t)} e^{-i\hat{V}_i(t+\Delta t)} e^{i\hat{V}_i(t)} e^{-E_i(t)} e^{-i\hat{V}_i(t)} \dots)$ can be rewritten in the limit $\Delta t \rightarrow 0$ as

$$Z_i = \text{Tr} \mathcal{T} e^{-\int_0^\beta (\hat{E}(t) + i \frac{\partial}{\partial t} \hat{V}(t)) dt} \quad (\text{S10})$$

The non-adiabatic term due rotating basis $i \frac{\partial}{\partial t} \hat{V}(t)$ acts as a perturbation. The lower-energy level, $E_\downarrow(t) = -\sqrt{\Gamma^2 + h_i^2(t)}$, makes a dominant contribution to the partition function in the limit $\beta \rightarrow \infty$. Including second-order correction from the perturbation theory, $|\partial V_{\downarrow\uparrow}/\partial t|^2/(E_\downarrow - E_\uparrow)$, one obtains:

$$\ln Z_i \approx \int_0^\beta \left(\sqrt{\Gamma^2 + h_i^2} - \frac{\Gamma^2 (\partial h_i / \partial t)^2}{8(\Gamma^2 + h_i^2)^{5/2}} \right) dt. \quad (\text{S11})$$

As the sum over all sites is performed, the first term in the integrand gives rise to a finite-size correction to the effective potential, which depends on angle ϑ and a particular realization of disorder

$$V_\Gamma(\vartheta) = - \sum_i \sqrt{\Gamma^2 + \xi_i^2 m_\Gamma^2 \sin^2(\vartheta - \theta_i)} + N \left\langle \sqrt{\Gamma^2 + \xi^2 m_\Gamma^2} \right\rangle_{\boldsymbol{\xi}}. \quad (\text{S12})$$

Vector-valued $\boldsymbol{\xi}_i$ has been parametrized here as $\xi_i \begin{pmatrix} \cos \vartheta(t) \\ \sin \vartheta(t) \end{pmatrix}$. Off-setting average in eqn. (S12) above has been made with respect to Gaussian distribution of the projection of $\boldsymbol{\xi}$ onto \mathbf{m} (its value is independent of the direction). The second term in the integrand of eqn. (S11) contributes

$$\int_0^\beta \sum_i \frac{\Gamma^2 \xi_i^2 m_\Gamma^2 \cos^2(\vartheta - \theta_i)}{8(\Gamma^2 + \xi_i^2 m_\Gamma^2 \sin^2(\vartheta - \theta_i))^{5/2}} dt = \int_0^\beta \frac{M}{2} \left(\frac{d\vartheta}{dt} \right)^2 dt. \quad (\text{S13})$$

The ‘effective mass’ M can be replaced by its average value

$$M = \frac{N m_\Gamma}{4\sqrt{2}\Gamma^2} U\left(-\frac{1}{2}; 1; \frac{\Gamma^2}{2m_\Gamma^2}\right), \quad (\text{S14})$$

which approaches $N/(4\sqrt{\pi}\Gamma^2)$ in the limit $\Gamma \rightarrow 0$. The dynamics becomes more classical as the effective mass diverges. Path integral (S6) is then rewritten as

$$Z \sim e^{-N\beta V(m_\Gamma)} \int [d\vartheta(t)] e^{-\int_0^\beta \left(\frac{M}{2} \left(\frac{d\vartheta}{dt} \right)^2 + V_\Gamma(\vartheta) \right) dt}. \quad (\text{S15})$$

The low-lying energy levels of the many-body problem are thus equivalent to those of a quantum mechanical particle on a ring.

The approximations made above break down for any finite N when Γ is sufficiently small. To avoid this, and to be able to make more quantitative predictions about the behavior of random potential (S12), it is necessary to study the continuous limit $N \rightarrow \infty$ directly.

Continuous Random Potential. Observe that the central limit theorem can be applied to the entire two-dimensional (in Γ and ϑ) process $V_\Gamma(\vartheta)$. This Gaussian process can be decorrelated by writing it as an infinite function series $V_\Gamma(\vartheta) = \sum_{n,m} \zeta_{nm} f_{nm}(\Gamma, \vartheta)$ involving independent Gaussian variables ζ_{nm} . Basis functions are determined from the covariance $\langle V_\Gamma(\vartheta) V_\Gamma(\vartheta') \rangle$. Since this correlation depends only on the angle difference $\vartheta - \vartheta'$, it is natural to use $f_{nm}(\Gamma, \vartheta) = \tilde{f}_{nm}(\Gamma) e^{im\vartheta}$.

Although the best truncated approximation is obtained by using Karhunen-Loève basis, there is no requirement that $\tilde{f}_{nm}(\Gamma)$ be orthogonal. In fact, since covariance involves averaging over distribution $\mathcal{P}(\xi) = \xi e^{-\xi^2/2}$, it is quite convenient to use a set of polynomials that are orthogonal with said weight. Using a set of white noise processes

$$\langle \zeta_n(\vartheta) \zeta_{n'}(\vartheta') \rangle = \delta_{nn'} \delta(\vartheta - \vartheta') \text{ for } \vartheta, \vartheta' \in [-\pi/2; \pi/2], \quad (\text{S16})$$

in lieu of discrete random variables, the series expansion becomes

$$V_\Gamma(\vartheta) = \sqrt{N} \sum_{n=0}^{\infty} \int_{-\pi/2}^{\pi/2} f_\Gamma^{(n)}(\vartheta - \theta) \zeta_n(\theta) d\theta, \quad (\text{S17})$$

where a factor \sqrt{N} had been introduced for convenience. The convolution kernels should be chosen so as to match the covariance. One suitable choice is

$$f_\Gamma^{(n)}(\vartheta) = A_n \int_0^\infty \sqrt{\Gamma^2 + m_\Gamma^2 \xi^2 \sin^2 \vartheta} \xi^{\alpha+1} e^{-\xi^2/2} L_n^{(\alpha)}\left(\frac{\xi^2}{2}\right) d\xi. \quad (\text{S18})$$

Since associated Laguerre polynomials form a complete orthogonal (with respect to weight $t^\alpha e^{-t}$ with $t = \xi^2/2$) set of basis function, it follows that

$$\sum_{n=0}^{\infty} f_\Gamma^{(n)}(\vartheta) L_n^{(\alpha)}\left(\frac{\xi^2}{2}\right) = \frac{2^\alpha \Gamma (n + \alpha + 1) A_n}{n! \xi^\alpha} \sqrt{\Gamma^2 + m_\Gamma^2 \xi^2 \sin^2 \vartheta}. \quad (\text{S19})$$

Representing $V_\Gamma(\vartheta)$ using ansatz of eqn. (S17) above one can write the expression for the covariance matrix. Using identities (S18) and (S19), it is transformed as follows:

$$\begin{aligned} \langle V_\Gamma(\vartheta) V_\Gamma(\vartheta') \rangle &= \sqrt{N} \sum_{n=0}^{\infty} \int_{-\pi/2}^{\pi/2} f_\Gamma^{(n)}(\vartheta - \theta) \langle \zeta_n(\theta) V_\Gamma(\vartheta') \rangle d\theta \\ &= N A_n \sum_{n=0}^{\infty} \int_{-\pi/2}^{\pi/2} f_\Gamma^{(n)}(\vartheta - \theta) \times \\ &\quad \int_0^\infty \sqrt{\Gamma'^2 + m_\Gamma^2 \xi^2 \sin^2(\vartheta' - \theta)} \xi^{\alpha+1} e^{-\xi^2/2} L_n^{(\alpha)}\left(\frac{\xi^2}{2}\right) d\xi d\theta \\ &= \frac{2^\alpha \Gamma (n + \alpha + 1) N A_n^2}{n!} \int_{-\pi/2}^{\pi/2} \int_0^\infty \sqrt{\Gamma^2 + m_\Gamma^2 \xi^2 \sin^2(\vartheta - \theta)} \times \\ &\quad \sqrt{\Gamma'^2 + m_\Gamma^2 \xi^2 \sin^2(\vartheta' - \theta)} \xi e^{-\xi^2/2} d\xi d\theta. \quad (\text{S20}) \end{aligned}$$

This matches the correct value obtained by replacing sum over sites by disorder averages and determines the normalization constant:

$$A_n = \sqrt{\frac{n!}{2^\alpha \pi \Gamma (n + \alpha + 1)}}. \quad (\text{S21})$$

Notice that the value of α can be chosen freely: as mentioned above, the decomposition is not unique. The most convenient choice, $\alpha = 1$, leads to the vanishing of all convolution kernels with $n \geq 1$ in the limit $\Gamma = 0$. Introducing the rescaled potential via $V_0(\vartheta) = (2\sqrt{N}/\pi)\chi(\vartheta)$, it is straightforward to verify that

$$\chi(\vartheta) = \int_{-\pi/2}^{\pi/2} \frac{1}{2} |\sin(\vartheta - \theta)| \zeta_0(\theta) d\theta \quad (\text{S22})$$

satisfies the following stochastic equation:

$$\frac{d^2 \chi}{d\vartheta^2} + \chi = \zeta_0(\vartheta). \quad (\text{S23})$$

The solution is determined uniquely by enforcing periodic boundary conditions: $\chi(-\pi/2) = \chi(\pi/2)$ and $\chi'(-\pi/2) = \chi'(\pi/2)$.

Now considering a finite $\Gamma > 0$, it becomes convenient to re-express $n = 0$ term in the functional series as a convolution with $\chi(\vartheta)$ instead. This can be accomplished by substituting the left hand side of (S23) into eqn. (S17) and performing integration by parts. Other terms can also be more conveniently expressed by rewriting white-noise processes in terms of continuous processes: realizations of periodic brownian motion

$$\frac{d\eta_n}{d\vartheta} + \bar{\zeta}_n = \zeta_n(\vartheta). \quad (\text{S24})$$

Here $\bar{\zeta}_n = \frac{1}{\pi} \int_{-\pi/2}^{\pi/2} \zeta_n(\vartheta) d\vartheta$ is added to ensure periodicity: $\eta_n(-\pi/2) = \eta_n(\pi/2)$.

Now, the random potential is rewritten as

$$V_\Gamma(\vartheta) = \sqrt{N} \frac{m_\Gamma}{\sqrt{\pi/2}} \left((f_\Gamma \star \chi)(\vartheta) + \sum_{n=1}^{\infty} (g_\Gamma^{(n)} \star \eta_n)(\vartheta) + \text{const} \right). \quad (\text{S25})$$

The last term is angle-independent random variable that absorbs $\{\bar{\zeta}_n\}$. Being a constant offset, it cannot affect the physics; and, thus, will be neglected. Expressions for kernels $f_\Gamma(\vartheta)$ and $g_\Gamma^{(n)}$ are obtained by performing integration by parts in variable ϑ :

$$f_\Gamma(\vartheta) = \int_0^\infty \frac{\tilde{\Gamma}^2 (\tilde{\Gamma}^2 + \xi^2) \xi^2}{2(\tilde{\Gamma}^2 + \xi^2 \sin^2 \vartheta)^{3/2}} e^{-\xi^2/2} d\xi, \quad (\text{S26})$$

$$g_\Gamma^{(n)}(\vartheta) = \frac{\sin \vartheta \cos \vartheta}{2\sqrt{n+1}} \int_0^\infty \frac{\xi^4 L_n^{(1)}\left(\frac{\xi^2}{2}\right)}{\sqrt{\tilde{\Gamma}^2 + \xi^2 \sin^2 \vartheta}} e^{-\xi^2/2} d\xi. \quad (\text{S27})$$

where the rescaled transverse field $\tilde{\Gamma} = \Gamma/m_\Gamma$ has been introduced for convenience. Using substitutions $t = \xi^2/2$ and $x = \tilde{\Gamma}^2/(2\sin^2 \vartheta)$, the integrals above can be converted to Mellin form and evaluated in terms of special functions:

$$f_\Gamma(\vartheta) = \frac{\sqrt{\pi} \tilde{\Gamma}^2}{8 \sin^3 \vartheta} \left[3U\left(\frac{3}{2}, 0; \frac{\tilde{\Gamma}^2}{2\sin^2 \vartheta}\right) + \tilde{\Gamma}^2 U\left(\frac{3}{2}, 1; \frac{\tilde{\Gamma}^2}{2\sin^2 \vartheta}\right) \right], \quad (\text{S28})$$

$$g_\Gamma^{(n)}(\vartheta) = \frac{\sqrt{\pi} \cos \vartheta}{\sqrt{n+1} n!} G_{2,3}^{2,2} \left(\frac{\tilde{\Gamma}^2}{2\sin^2 \vartheta} \middle| \begin{matrix} 1-n, \frac{1}{2} \\ 1, 2; 0 \end{matrix} \right). \quad (\text{S29})$$

Tunneling gaps are associated with global bifurcations of $V_\Gamma(\vartheta)$ which occur mostly in the limit $\Gamma \ll 1$. Moreover, it is this limit that is governed by universal scaling laws and thus will be investigated in greater detail. The kernels above act on scales $\vartheta \sim \Gamma$. For small Γ it is permissible to drop the second term in eqn. (S28) and to replace $\sin \vartheta \approx \vartheta$ and $\cos \vartheta \approx 1$ everywhere. It will be seen that any bifurcations also take place for $\vartheta \sim \Gamma$, hence the periodicity of the potential $V_\Gamma(\vartheta)$ becomes irrelevant.

Extremal Statistics. The distribution of bottlenecks in the limit $\Gamma \ll 1$ is related to the properties of the classical potential $\chi(\vartheta)$ in a proximity of its global minimum ϑ_0^* . It will be governed by different statistics, derived below, by virtue of this extremality condition.

On short scales, the linear term on the left hand side of eqn. (S23) can be neglected in comparison with the large stochastic term

$\zeta_0(\vartheta)$. It will be seen self-consistently that the relevant range is $|\vartheta - \vartheta_0^*| = O(\Gamma)$. The stochastic equation describes a free particle in 1D subjected to random force. Specifying the ‘coordinate’ χ together with the ‘velocity’ $v = d\chi/d\vartheta$ for some ϑ determines their distribution either in the ‘future’ ($\vartheta' > \vartheta$) or in the ‘past’ ($\vartheta' < \vartheta$), where ϑ plays the role of time. This can be described by the following PDE:

$$\frac{\partial p}{\partial \vartheta} + v \frac{\partial p}{\partial \chi} - \frac{1}{2} \frac{\partial^2 p}{\partial v^2} = 0, \quad (\text{S30})$$

where $p(\vartheta; \chi, v)$ is the probability density. It will be convenient to perform a shift so that a global minimum coincides with the origin: $\vartheta_0^* = 0$ and $\chi(0) = 0$. Another condition is necessary to ensure that $\chi(\vartheta) > 0$ for $\vartheta \neq 0$. Considering only $\vartheta > 0$ for concreteness, one may introduce an absorbing boundary via boundary condition

$$\lim_{\chi \rightarrow +0} p(\vartheta; \chi, v) = 0 \quad \text{for } v > 0. \quad (\text{S31})$$

Notice that the probability need not vanish as $\chi \rightarrow +0$ for negative velocities $v < 0$. The probability that a random path does not hit this boundary decays as follows:

$$\frac{\partial}{\partial \vartheta} \int p(\vartheta; \chi, v) d\chi dv = \int_{-\infty}^0 v p(\vartheta; +0, v) dv. \quad (\text{S32})$$

Since the random process is conditioned on the fact that it starts at a global minimum, it is convenient to ‘renormalize’ the probability so that it becomes a conserved quantity once again. Consider a probability that χ stays positive at least until some distant horizon Θ ,

$$q(\vartheta; \chi, v) \propto p(\vartheta; \chi, v) \underbrace{\int_{\Theta > 0} P(\Theta; X, \Upsilon | \vartheta; \chi, v) dX d\Upsilon}_{P_{\Theta}(\chi, v, \vartheta)}, \quad (\text{S33})$$

with an appropriate normalization factor. The second factor, $P_{\Theta}(\vartheta; \chi, v)$ represents the survival probability. It is written as an integral of the Green’s function associated with eqn. (S30). Time-reversal symmetry implies

$$P(\Theta; X, \Upsilon | \vartheta; \chi, v) = P(\vartheta; \chi, -v | \Theta; X, -\Upsilon). \quad (\text{S34})$$

As a result $P_{\Theta}(\vartheta; \chi, v)$ satisfies a PDE obtained from eqn. (S30) by changing the sign of $\frac{\partial v}{\partial \vartheta}$ and $v \frac{\partial p}{\partial \chi}$. With this in mind, the equation for renormalized probability becomes

$$\frac{\partial q}{\partial \vartheta} + v \frac{\partial q}{\partial \chi} + \frac{\partial}{\partial v} \left(\frac{1}{P_{\Theta}} \frac{\partial P_{\Theta}}{\partial v} q \right) - \frac{1}{2} \frac{\partial^2 q}{\partial v^2} = 0. \quad (\text{S35})$$

In comparison with eqn. (S30), it adds a drift $\propto \partial(\log P_{\Theta})/\partial v$ in addition to the diffusion of ‘velocity’ v .

In the limit of large Θ , the ‘survival’ probability $P_{\Theta}(\chi, v, \vartheta)$ corresponds — up to time-reversal ($v \rightarrow -v$) — to the asymptotic solution of (S30),

$$p(\chi, v, \vartheta) \sim A \frac{p_*(\chi, v)}{\vartheta^\alpha}. \quad (\text{S36})$$

Probability density always converges to this form as $\vartheta \rightarrow \infty$, with dependence on the initial conditions only via the prefactor A . Here $p_*(\chi, v)$ can be thought of as a ‘stationary’ solution: it satisfies eqn. (S30) (with $\partial/\partial \vartheta$ term dropped) and boundary condition (S31). Eqn. (S30) is invariant with respect to rescaling $(\vartheta, \chi, v) \mapsto (\ell \vartheta, \ell^{3/2} \chi, \ell^{1/2} v)$. For this reason, the asymptotic solution should be sought in the form

$$p_*(\chi, v) = \chi^{2\alpha/3} p_*(v/\chi^{1/3}). \quad (\text{S37})$$

It is possible to simplify equations even further by introducing new ‘dimensionless’ variables. Defining new ‘time’ variable via

$d\tau = d\vartheta/\chi^{2/3}$, it is now a triple (ϑ, χ, v) that becomes new Markov process. This modification merely adds $\chi^{-2/3}(\partial q/\partial \tau) + \frac{2}{3}(v/\chi)q$ to the left hand side of eqn. (S35). The term $\propto q$ reflects renormalization of probability density as a result of non-linear transformation.

Furthermore, it is convenient to introduce new ‘dimensionless’ velocity $\nu = v/\chi^{1/3}$ and the ‘logarithmic’ coordinate $\mu = \ln \chi$. The new probability density, appropriately renormalized, reads

$$\bar{q}(\tau; \vartheta, \mu, \nu) = e^{4\mu/3} q(\tau; \vartheta, e^\mu, \nu e^{\mu/3}). \quad (\text{S38})$$

This is substituted into eqn. (S35) which has been modified as described in the previous paragraph. Replacing $\partial/\partial \chi \mapsto e^{-\mu}(\partial/\partial \mu - \frac{1}{3}\nu \partial/\partial \nu)$ and $\partial/\partial v \mapsto e^{-\mu/3} \partial/\partial \nu$, the following PDE is obtained:

$$\frac{\partial \bar{q}}{\partial \tau} + e^{2\mu/3} \frac{\partial \bar{q}}{\partial \vartheta} + \nu \frac{\partial \bar{q}}{\partial \mu} - \frac{\partial}{\partial \nu} \left(\frac{\partial \mathcal{U}}{\partial \nu} \bar{q} \right) - \frac{1}{2} \frac{\partial^2 \bar{q}}{\partial \nu^2} = 0, \quad (\text{S39})$$

where the non-linear potential is written, using eqn. (S37), as

$$\mathcal{U}(\nu) \sim \frac{\nu^3}{9} - \ln p_*(-\nu). \quad (\text{S40})$$

When $p(\tau; \vartheta, \mu, \nu)$ is marginalized over ϑ, μ , the standard Fokker-Planck equation is obtained. It describes a stochastic process

$$\frac{d\nu}{d\tau} = -\mathcal{U}'(\nu) \text{sgn } \tau + \zeta(\tau), \quad (\text{S41})$$

where $\zeta(\tau)$ is the white-noise random force. This stochastic equation can be integrated both forward ($\tau > 0$) and backwards ($\tau < 0$) starting from $\nu(0)$ drawn from the equilibrium distribution $\rho(\nu) \propto e^{-2\mathcal{U}(\nu)}$.

To find the shape of $\mathcal{U}(\nu)$ and $\rho(\nu)$, observe that $p_*(v/\chi^{1/3})$ satisfies a stationary version of eqn. (S30), which is reduced to ordinary differential equation. Writing $z = \nu^3/9$,

$$z\psi'' + \frac{2}{3}\psi' + \left(\frac{2+4\alpha}{3} - z \right) \psi = 0, \quad (\text{S42})$$

where $\psi(z) = \sqrt{\rho(z)}$. Disallowing exponentially increasing solutions, $\psi(z)$ is sought in the form $e^{\mp z} f_{\pm}(z)$ for $z > 0$ and $z < 0$ respectively. This substitution transforms eqn. (S42) to hypergeometric form, giving the two branches as $f_+(z) \propto U(-\frac{2\alpha}{3}; \frac{2}{3}; 2z)$ and $f_-(z) \propto U(\frac{2}{3} + \frac{2\alpha}{3}; \frac{2}{3}; -2z)$. Matching logarithmic derivatives

$$\frac{\psi'(+0)}{\psi(+0)} = -A \frac{\Gamma(\frac{1}{3} - \frac{2\alpha}{3})}{\Gamma(-\frac{2\alpha}{3})} \quad \text{and} \quad \frac{\psi'(-0)}{\psi(-0)} = A \frac{\Gamma(1 + \frac{2\alpha}{3})}{\Gamma(\frac{2}{3} + \frac{2\alpha}{3})} \quad (\text{S43})$$

[where the common factor is $A = 3^{1/3} \Gamma(\frac{2}{3})/\Gamma(\frac{1}{3})$] requires that

$$\alpha = \frac{1}{4} + \frac{3}{2}n, \quad (\text{S44})$$

as verified using of Euler’s identity $\Gamma(x)\Gamma(1-x) = \pi/\sin(\pi x)$. Of this infinite set, the smallest positive value $\alpha = 1/4$ has to be chosen. The analytical expression that defines the potential $\mathcal{U}(\nu)$ can be simplified as follows:

$$\psi(\nu) \propto e^{-\mathcal{U}(\nu)} = x \text{Ai}(x^2) - \text{Ai}'(x^2), \quad \text{where } x = \nu/\sqrt[3]{6}. \quad (\text{S45})$$

Since eqn. (S39) is first order in ϑ, μ , these are completely deterministic, given a particular realization of stochastic process (S41):

$$\frac{d\mu}{d\tau} = \nu(\tau), \quad (\text{S46})$$

$$\frac{d\vartheta}{d\tau} = \chi^{2/3}(\tau), \quad (\text{S47})$$

with boundary conditions $\chi(-\infty) = \vartheta(-\infty) = 0$. This procedure defines the process $\chi(\vartheta)$ parametrically. So far, a positive branch ($\vartheta > 0$) had been considered. Negative branch ($\vartheta < 0$) is obtained similarly; positive and negative branches are uncorrelated.